



# Enhancing Physical-Layer Key Generation Accuracy through Deep Learning-Based Hardware Calibration

Yawen Zheng, Xu Wang, Fan Dang, Xin Miao

Tsinghua University

yw-zheng21@mails.tsinghua.edu.cn,{xu\_wang,dangfan,miaoxin}@tsinghua.edu.cn

## Abstract

This paper introduces a deep learning-based approach for calibrating hardware defects in physical-layer key generation (PKG) tasks, focusing on directional-of-arrival (DoA) based key generation in wireless communication systems. The proposed scheme leverages a novel neural network architecture, incorporating residual and self-attention mechanisms, to accurately map spatial features under coherent signals, thereby significantly reducing bit mismatch rates inherent to antenna array imperfections. Through extensive simulation experiments, the method demonstrates improved robustness and effectiveness over traditional calibration techniques and existing deep-learning models, particularly in environments characterized by defect complexity and signal coherence challenges. Our findings offer a promising avenue for enhancing the security of wireless communications by optimizing the performance of PKG solutions.

**CCS Concepts:** • Security and privacy → Mobile and wireless security; • Computing methodologies → Neural networks.

**Keywords:** Hardware Calibration, Physical-layer Key Generation, Deep Learning

## ACM Reference Format:

Yawen Zheng, Xu Wang, Fan Dang, Xin Miao. 2024. Enhancing Physical-Layer Key Generation Accuracy through Deep Learning-Based Hardware Calibration. In *Workshop on Adaptive AIoT Systems (AdaAloTSys '24), June 3–7, 2024, Minato-ku, Tokyo, Japan*. ACM, New York, NY, USA, 6 pages. <https://doi.org/10.1145/3662007.3663883>

## 1 Introduction

Physical-layer key generation (PKG) has emerged as a promising solution for enhancing the security of wireless communications [19]. Traditional PKG methods typically comprise several steps: channel probing and estimation, quantization,

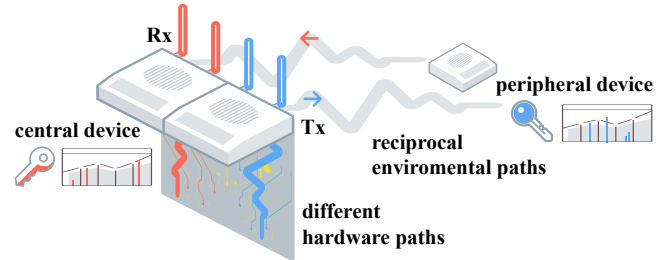


**Figure 1.** Hardware defects jeopardize the channel reciprocity required for Physical-layer key generation.

information reconciliation, and privacy amplification. The characteristics extracted from communication channels vary with specific protocols and devices, encompassing the Received Signal Strength Indicator (RSSI), Channel State Information (CSI), and Direction of Arrival (DOA), among others.

Common PKG approaches in wireless communications predominantly focus on the channel reciprocity between legitimate devices and spatial decorrelation with eavesdropping devices. However, most studies have concentrated on the signal propagation paths through the spatial environment, neglecting the "paths" related to hardware components such as the transmitting and receiving circuits and physical antennas, as is illustrated in figure 1. Due to manufacturing imperfections in its components, hardware may exhibit significant variations in key device parameters across production batches, inducing unique variations in the physical layer IQ signals. Researchers have leveraged such distinctive fingerprints as a physical basis for device authentication [4, 14]. However, when hardware is considered an integral part of the wireless communication channel, these specific hardware imperfections could interfere with the channel characteristics captured by two legitimate devices, thereby increasing the mismatch rate of the generated raw key bits.

This is particularly true for PKG tasks relying on antenna arrays, where dissimilar defects among different physical antennas and circuit components can impair accurate measurement and computation of channel differences among antennas. Notably, while the information reconciliation phase in PKG can mitigate smaller errors, the information leakage rates of commonly used Cascade protocols and BCH error-correcting codes are typically higher than the actual bit error rates [6], resulting in a greater loss of information entropy



This work is licensed under a Creative Commons Attribution-NonCommercial-ShareAlike International 4.0 License.

*AdaAloTSys '24, June 3–7, 2024, Minato-ku, Tokyo, Japan*

© 2024 Copyright held by the owner/author(s).

ACM ISBN 979-8-4007-0664-6/24/06

<https://doi.org/10.1145/3662007.3663883>

than the erroneous bits themselves. Hence, the most desirable solution remains to minimize the mismatched raw bits during the channel estimation and quantization stages. Addressing this phenomenon, existing works often implement additional calibration steps in the experimental setup phase, such as utilizing time synchronization methods to eliminate CFD and clock biases, thereby approximating hardware to ideal conditions. However, in real-world scenarios, errors induced by hardware imperfections can be multifactorial, nonlinear, and variant with different array geometry, which is challenging to characterize with a general explicit model.

**Table 1. Comparisons of current works**

Challenges	Defect complexity	Signal coherence	Spectrum dependency
KGNet [20]	✗	✓	N/A
DNN-based DF [10]	✓	✗	✓
CNN-based DF [13]	✗	✓	✗
Our approach	✓	✓	✓

As is shown in Table 1, deep learning methods have been introduced to enhance the mapping of channel features in PKG tasks [20], but it remains an open issue to transfer the environmental-adaptive model to diverse defective hardware. Although imperfections of antenna arrays have been noticed in the domain of Direction Finding (DF) [10], the proposed DNN-based approach employs simulations by superimposing multiple incoherent signal sources, which neglects the fact that coherent multi-path signal propagations serve as the primary source of entropy in DOA-based PKG tasks. Another CNN-based solution contributes to resolving the discrete directions of coherent signals [13], but for PKG tasks, utilizing the entire spatial spectrum for fine-grained extraction of reciprocal information is essential to maximize key generation rates. Consequently, tackling PKG tasks with antenna array hardware defects presents challenges related to defect complexity, signal coherence, and spatial spectrum dependency, which current studies have not comprehensively addressed.

This paper proposes a deep learning-based calibration scheme designed to eliminate errors caused by hardware defects while extracting multi-antenna channel information, thereby optimizing the accuracy of DOA-based PKG tasks sensitive to spatial features. Our contributions include:

- We leveraged a deep-learning solution to calibrate hardware defects, thereby reducing the original bit mismatching rate of PKG tasks.
- We introduced residual and self-attention structures to map spatial features under coherent signals across different array manifolds.
- We validated the effectiveness and robustness of our approach through simulation experiments.

## 2 Methods

### 2.1 Problem Formulation

Central device A and peripheral device B constitute a pair of legitimate entities in a wireless communication system, where the central device is equipped with an antenna array consisting of  $M$  elements, and the peripheral device is equipped with a single antenna.

In the process of PKG, device A schedules its antenna array to transmit a signal  $s(t)$  to device B. After being reflected by obstacles in the environment, this signal is received by device B as a superposition of  $N$  multipath propagations. Similarly, at time  $t'$  (where both  $t$  and  $t'$  fall within the same coherence time), device B transmits a signal  $s'(t')$  back to device A, which is then received by the antenna array following the same propagation paths. Devices A and B each employ a direction-finding algorithm to compute the spatial spectrum distribution of the received signals and then quantize it to generate a raw bit sequence. Subsequently, through information reconciliation and privacy amplification steps, the two devices produce a consistent secret key separately.

The signal  $\mathbf{r}(t)$  received by device B with ambient noises  $\mathbf{n}(t)$  can be represented as follows:

$$\mathbf{r}(t) = \sum_{n=1}^N \alpha_n e^{j\phi_n} \mathbf{A}(\theta_n) s(t - \tau_n) + \mathbf{n}(t), \quad (1)$$

where  $\alpha_n$ ,  $e^{j\phi_n}$ ,  $\theta_n$  and  $\tau_n$  are the different path loss, phase shift, direction angle, and time delay for the  $n$ th path.  $\mathbf{A}(\theta)$  is the steering vector of the antenna elements. For an ideal uniform linear array, an element  $a_m$  of  $\mathbf{A}(\theta_n)$  (representing the response of the  $m$ th antenna to the  $n$ th path) can be specifically expressed as:

$$a_m = e^{-j\frac{2\pi}{\lambda} d_m \sin(\theta_n)}, \quad (2)$$

where  $d_m$  indicates the relative position of the  $m$ th antenna element, and  $\lambda$  is the wavelength of the signal. The signal  $\mathbf{r}'(t)$  received by the central device characterized by  $\mathbf{A}'(\theta)$  can be derived in a similar manner.

Theoretically, the spatial features extracted from the received signal  $\mathbf{r}'(t)$  by device A should be reciprocal to those extracted from  $\mathbf{r}(t)$  by device B. However, the steering vectors in the expression for  $\mathbf{r}(t)$  apply to the array manifold of the transmitter RF chains, whereas the steering vectors for  $\mathbf{r}'(t)$  depend on that of the receiver RF chains. For real-world implementations, the antenna manifold is subject to distortions due to various imperfections inherent in the physical antennas and the transmitting/receiving circuits. These distortions lead to discrepancies between the spatial distribution of signals received by devices A and B, which further induces a higher bit mismatch rate.

This work aims to establish a mapping function between the two, thereby reducing the mismatch rate of the raw key

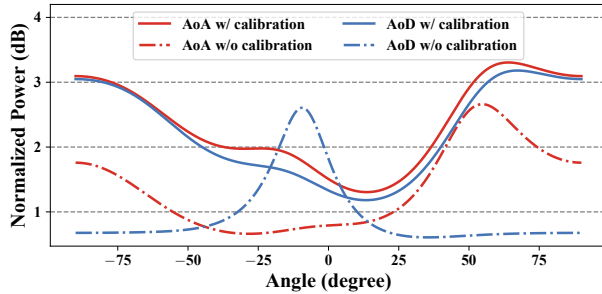


**Figure 2.** Calibration of antenna arrays is essential to extract the reciprocal spatial channel features correctly.

bits, which can be represented as follows:

$$\mathbf{G} = \arg \min_{\mathbf{G}} \|\mathbf{A}(\theta) - \mathbf{G}(\mathbf{A}'(\theta))\|_F, \quad (3)$$

where  $\mathbf{G}$  minimizes the Frobenius norm of the difference between the steering matrices. However, as in practical scenarios, the steering matrices are agnostic. Therefore, we utilize the signal covariance matrix

$$\mathbf{R} = E[\mathbf{r}(t)\mathbf{r}(t)^H] = \mathbf{A}(\theta)\mathbf{S}\mathbf{A}(\theta)^H + \sigma^2\mathbf{I} \quad (4)$$

to approximate the sought  $\mathbf{G}$ :

$$\hat{\mathbf{G}} = \arg \min_{\mathbf{G}} \|\mathbf{R} - \mathbf{G}(\mathbf{R}')\|_F, \quad (5)$$

where  $\mathbf{S}$  is a diagonal matrix containing the power of signals  $\mathbf{s}(t)$  in each direction,  $\sigma^2$  represents the variance of noises and  $\mathbf{R}'$  is the signal covariance matrix of  $\mathbf{r}'(t)$ .

Notably, the departure angle of the signals from the central device and the arrival angle of the signals to the central device constitute the reciprocity of the spatial spectrum. Consequently, the defect calibration method discussed in this paper pertains solely to the central device's antenna manifold in both its transmitting and receiving modes of operation. Such an assumption is reasonable because specifications are provided for angle of departure (AoD) and angle of arrival (AoA) measurement interfaces for commonly used wireless communication protocols such as BLE 5.1 [17]. In addition, antenna array hardware is not required for the peripheral device, and additional calibration steps are not needed.

## 2.2 Preliminary: Antenna Array Defects

Ideally, the shape of the array manifold is determined by the design of the antenna array [2]. However, imperfections in physical antennas and the transmitting/receiving circuits can distort it, thereby affecting the ability of the central device to perceive spatial characteristics.

We established a three-element antenna array with COTS USRP N210s, and figure 2 illustrates the AoA and AoD spatial spectra calculated respectively by the central and peripheral devices before and after calibration (by modifying hardware connection states as in figure 3) of the central device. The



**Figure 3.** Traditional calibration methods may involve changing the connection state of the hardware.

disparities between the central device's transmitting and receiving RF chains threaten the basic channel reciprocity of PKG tasks. Defects embedded within the array may include:

**Element Imbalance.** Feeding imbalance among array elements causes aberrant manifold extension, leading to incorrect signal spatial characteristics mapping. Extreme events like packet loss in antenna arrays constructed with a single RF chain can even fail certain array elements [5].

**Mutual Coupling.** Mutual coupling in an array refers to one antenna element's influence on its neighboring elements' electromagnetic field, which is inevitable for a MIMO system [1]. This influence changes the input impedance, radiation pattern, and gain characteristics of the neighboring elements, causing distortions in the antenna array manifold.

**Phase Shift Errors.** In the case of antenna arrays composed of multiple RF chains, phase errors among different elements may arise due to variations of initial phase differences across the RF circuits. For hardware such as USRPs, such phase shift errors are attributable to the random initial state of a delta-sigma modulator in the FracN divider PLL [21].

The current methods for mitigating defect errors primarily involve collecting samples and calibrating the antenna manifold based on the transfer matrix through least squares estimation (under linear assumptions) [15]. More cumbersome methods may rely on special hardware modifications or enhancements. Unfortunately, according to Lee [11], defects like the mutual coupling between transmitting and receiving arrays generally differ; hence, distinct parameters should be employed for their analysis and compensation.

This paper aims to utilize deep learning to perform sample-based nonlinear mapping calibration for antennas of various shapes. Given that defects in various hardware components are often independent and cumulative, we simulate the signal based on various antenna defect models proposed in previous research, thereby generating datasets.

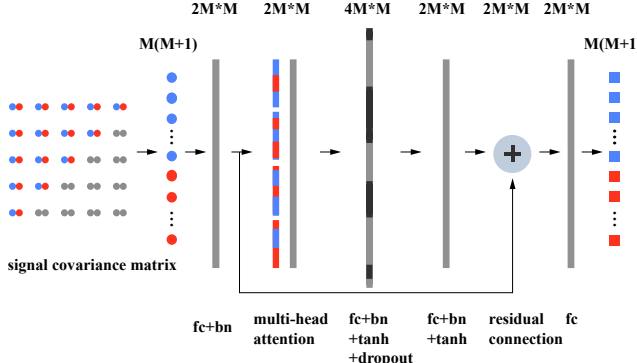


**Figure 4.** Network architecture of our approach, denoting the category of each layer and the dimension of features.

### 2.3 System Design

**Data preprocessing.** We firstly initialize two defective array manifolds  $\mathbf{A}(\theta)$  and  $\mathbf{A}'(\theta)$  based on the prior knowledge in 2.2, representing the transmitting or receiving antenna array of the central device respectively. Then, a randomized  $s(t)$  is simulated to propagate along different paths and produce a superimposition of the coherent signals with ambient noises.

Then, the signal covariance matrix  $\mathbf{R}$  and  $\mathbf{R}'$  is calculated based on the defective array manifolds and multi-path coherency, which is invariably symmetric. Therefore, we re-arrange the matrix by extracting only the upper triangular (including diagonal) elements to reduce data redundancy and stack the real and imaginary parts of each element, as in

$$\mathbf{v} = \begin{bmatrix} \Re(\mathbf{R}_{i,j}) \\ \Im(\mathbf{R}_{i,j}) \end{bmatrix}, 1 \leq i \leq j \leq n. \quad (6)$$

Lastly, we normalized the elements of  $\mathbf{v}$  to a distribution with a mean of 0 and a variance of 1. The data corresponding to the defective manifold  $\mathbf{A}'(\theta)$  serves as the label for the data corresponding to  $\mathbf{A}(\theta)$ .

**Network architecture.** We propose a novel neural network architecture tailored for processing structured covariance data, harmonizing linear and non-linear transformations to map between input data and corresponding labels adeptly for coherent multi-path signals, as is shown in figure 4.

According to 2.2, some array defects can be approximated to a linear transfer matrix, while others are generally considered nonlinear. In response to this feature, we implemented a residual connection that sums the linear output of the first fully connected layer and the nonlinear output of another. The residual block also alleviates the degradation problem and enhances the flow of gradients throughout the network.

Furthermore, we incorporate a self-attention mechanism to deal with coherent multi-path signals. Specifically, the roles of the signal covariance matrix elements are twofold in differentiating spatial features. The diagonal elements represent the power of individual signal components, while the

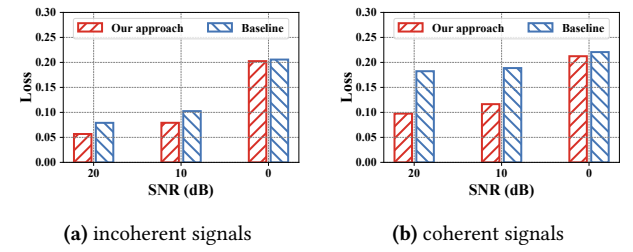


**Figure 5.** Impacts of signal coherence.

off-diagonal elements reflect the correlation between different components and are thus more sensitive to the coherency among signals. With the attention layer, the network can dynamically and context-sensitively prioritize the most salient features and capture their intricate dependencies.

**Physical-layer key generation.** PKG methods in [21] are adopted to evaluate how the calibrated signals lower the raw bit mismatch rate (BMR). We utilize a noise-maximized MUSIC algorithm to post-process the reconstructed signal co-variance matrix and quantize the spatial spectrum with Orthogonal polynomials. The steps for information reconciliation and privacy amplification are not within our scope.

## 3 Evaluation

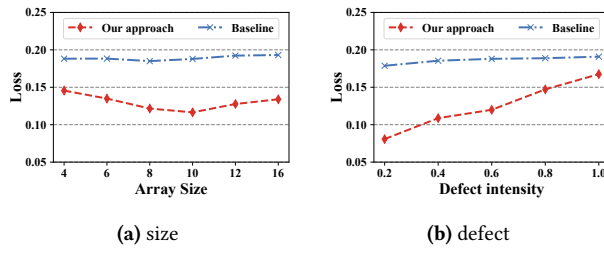
### 3.1 Simulation setups

In the simulation experiment setup, random signals  $s(t)$  are generated by a pairwise combination of angles, propagating along two paths corresponding to  $\alpha$  and  $\beta$ , resulting in superimposed signals. A two-layer traversal scan is conducted within  $[-60^\circ, 60^\circ]$ , each producing five samples with distinct environmental noises. Subsequently, datasets and corresponding label sets are constructed according to the methodology outlined in 2.3. Training is performed using the Adam optimizer and Mean Squared Error (MSE) loss function, with a batch size of 32 samples for 50 epochs.

### 3.2 Results

**Signal Coherence.** We compare our approach with DNN-based DF [10] as the baseline and examine the processing ability of coherent superimposed signals in conditions of different SNRs. The incoherent datasets are generated without multi-path data augmentation using a single-layer traversal scan across the targeted angle domains. In addition, we use a 10-element ULA, which is the same as the settings in [10].

As shown in figure 5a and 5b, our approach only marginally outperforms the baseline in scenarios with incoherent signals. On the other hand, it significantly betters the baseline for coherent signal ensembles, reducing loss in terms of RMSE by 28.2% and 22.8% at SNRs of 20dB and 10dB. Besides, as the database is generated based on signal covariance matrices without denoising, the performance of both methods

**Figure 6.** Impacts of hardware disparities.

noticeably decreases in low SNR (SNR=0 indicates the noise is of equal strength to the signals) scenarios.

**Hardware Adaptation.** We further investigated the impact of hardware disparities on network performance in coherent signal scenarios at a fixed SNR of 10 dB.

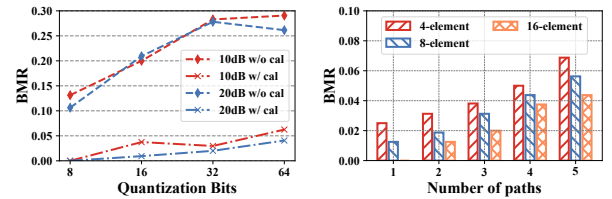
For different sizes of antenna arrays, we conducted tests within a range of element numbers in various settings of previous works [5, 10, 13]. It can be observed that the losses of both our methods and the baseline initially decrease and then increase with the increase in the number of elements, reaching their minimum at element numbers of 8 and 10, respectively. This may be attributed to the signal data being reinforced with increased elements in the initial phase, which benefits network training. However, in the later stages, the antenna manifold defects become increasingly challenging to fit due to differences between elements. Nevertheless, overall, our method outperforms the baseline across typical numbers of elements in antenna arrays.

Various hardware impairments were examined by utilizing a defect intensity parameter  $\omega$  to control the degree of distortion to the antenna manifold, ranging from minimal distortion (when  $\omega = 0$ , representing an undistorted manifold) to significant impairments such as failed elements, phase shifts up to  $\pi/3$ , and mechanical misalignments of half a wavelength at array spacings (when  $\omega = 1$ ). As is shown in figure 6b, our method exhibits significantly lower losses compared to the baseline when the manifold distortion is relatively mild, which corresponds to most real-world scenarios. As the degree of distortion increases, the loss approaches but consistently remains below that of the baseline.

### PKG Performance.

We employed the PKG workflow from [21] to assess the performance of our calibration method. For a 10-element array, we computed the bit mismatch rate (BMR) when quantizing a single spectrum into raw bit sequences of different lengths under relatively high and low SNRs.

As illustrated in figure 7, our calibration method significantly reduces the BMR by an absolute 20%–30% without compromising the key generation rate (BGR). Besides, the BMR of our method slightly grows with the increase in quantization length (following a trend similar to the uncalibrated

**Figure 7.** Impacts of raw bit sequence length.**Figure 8.** Generalization to multi-path environments.

baseline but with a notably smaller magnitude), and noise also marginally elevates the BMR. Yet, it remains below 5% in almost all the tested scenarios.

### Environment Generalization.

While generating simulated databases for training the network, we employ a data augmentation method that only utilizes signals superimposed along two distinct dominant paths. Subsequently, we conducted further tests to assess the generalization capability of the trained network for different quantities of multipath signals in PKG tasks. Additionally, simulations were conducted for 3 common antenna array configurations, which also impact spatial resolution.

As depicted in the figure 8, despite being trained on a 2-path database, the network demonstrates proficient calibration capabilities in extracting spatial features from signals propagated along 1 to 5 multipath routes. Moreover, for most test scenarios (except for complex cases involving the superposition of 5-path signals), it effectively reduces the BMR to below 5%. Notably, increasing the number of antenna array elements enhances PKG performance in this case.

## 4 Discussion

**Hardware co-design.** In this work, we regard the impacts of hardware defects on antenna manifolds as a fixed mapping function. However, in reality, factors such as hardware clock offsets and phase discontinuities may be subject to time-varying influences such as temperature. To thoroughly analyze the impact of hardware on algorithm implementation, a hardware and software co-design approach is essential.

**Task migration.** This study only investigates the effectiveness of deep learning-based calibration methods using DOA-based PKG methods as a case study. However, our approach can be easily transferred to various other subtasks, including direction finding, beamforming, wireless sensing, etc.

## 5 Related Work

**PKG Based on Spatial Features.** Considerable work has utilized similar spatial channel characteristics gathered from legitimate devices to extract keys from physical-layer information. The most universal approach is based on wireless channel reciprocity, with two devices exchanging featured

signals in a shared physical ambient environment [9, 21]. Some researchers generate secret keys among neighboring devices with similar spatial backgrounds, exerting unique features such as the echo profiles of acoustic signals [7] and environmental electromagnetic radiation extracted from RF signals [8]. For groups of devices in a broader neighboring spatial domain, the time intervals between continuous device events have been used as a source of entropy [3].

However, previous works either overlook the variations introduced by signals passing through different circuits and antennas, or involve cumbersome calibration which changes the operational state of devices. In contrast, our approach calibrates device hardware defects through a data-driven method, reducing errors in wireless channel reciprocity without necessitating additional hardware modifications.

**AI for Signal Processing Enhancement.** Data-driven approaches have been widely leveraged to enhance wireless techniques, addressing issues difficult to model and resolve through traditional algorithms. With such progress in data processing or generation, a wide scope of tasks based on wireless techniques produces better performances, including Direction Finding [10, 13], localization [16] and Physical-layer Key Generation [20].

Notably, it is equally significant to push forward the implementation of AI on embodied hardware entities with various manufacturing limitations [12, 18]. This paper proposes using neural networks to address the decline in channel reciprocity and increased bit mismatch rates caused by hardware defects for PKG tasks, and corresponding optimizations are made for defect complexity and signal coherence.

## 6 Conclusion

In conclusion, this study presents a pioneering deep-learning solution for addressing hardware defects in DOA-based PKG tasks, effectively bridging the gap between the ideal and practical performance of wireless communication systems.

By ingeniously incorporating residual connections and self-attention structures, our approach not only corrects for hardware-induced discrepancies in channel estimation and quantization but also sets a new benchmark for the accuracy and efficiency of PKG processes. The extensive simulation results underscore the superiority of our method in various challenging scenarios, highlighting its potential to significantly enhance the security and reliability of wireless communications. Future work will focus on extending this methodology to a broader range of communication protocols and hardware configurations, further solidifying the practical impact of deep learning in securing wireless networks.

## Acknowledgments

This work is supported in part by the National Key R&D Program of China under grant No. 2021YFB2900100.

## References

- [1] Xiaoming Chen, Shuai Zhang, and Qinlong Li. 2018. A review of mutual coupling in MIMO systems. *IEEE Access* 6 (2018), 24706–24719.
- [2] Georgios Efstathopoulos and Athanassios Manikas. 2011. Extended array manifolds: Functions of array manifolds. *IEEE Trans. Signal Process.* 59, 7 (2011), 3272–3287.
- [3] Habiba Farrukh, Muslum Ozgur Ozmen, Faik Kerem Ors, and et al. 2023. One key to rule them all: Secure group pairing for heterogeneous IoT devices. In *Proc. of IEEE S&P'23*. 3026–3042.
- [4] Hadi Givehchian, Nishant Bhaskar, Alexander Redding, and et al. 2023. Practical Obfuscation of BLE Physical-Layer Fingerprints on Mobile Devices. In *Proc. of IEEE S&P'23*. 73–73.
- [5] Zhihao Gu, Taiwei He, Junwei Yin, and et al. 2021. TyrLoc: a low-cost multi-technology MIMO localization system with a single RF chain. In *Proc. of ACM MobiSys'21*. 228–240.
- [6] Christopher Huth, René Guillaume, Thomas Strohm, and et al. 2016. Information reconciliation schemes in physical-layer security: A survey. *Comput. Netw.* 109 (2016), 84–104.
- [7] Meng Jin and Xinbing Wang. 2022. Pairing IoT devices with spatial keys. In *Proc. of ACM/IEEE IPSN'22*. 171–182.
- [8] Kyuin Lee, Yucheng Yang, Omkar Prabhune, and et al. 2022. AEROKEY: Using ambient electromagnetic radiation for secure and usable wireless device authentication. In *Proc. of ACM IMWUT'22*, Vol. 6. 1–29.
- [9] Guyue Li, Lei Hu, Paul Staat, and et al. 2022. Reconfigurable intelligent surface for physical layer key generation: Constructive or destructive? *IEEE Wirel. Commun.* 29, 4 (2022), 146–153.
- [10] Zhang-Meng Liu, Chenwei Zhang, and S Yu Philip. 2018. Direction-of-arrival estimation based on deep neural networks with robustness to array imperfections. *IEEE Trans. Antennas Propag.* 66, 12 (2018), 7315–7327.
- [11] Hoi-Shun Lui, Hon Tat Hui, and Mook Seng Leong. 2009. A note on the mutual-coupling problems in transmitting and receiving antenna arrays. *IEEE Antennas Propag. Mag.* 51, 5 (2009), 171–176.
- [12] Ji Luo, Yiling Hu, Chengzhao Yu, and et al. 2023. Field Reconstruction-Based Non-Rendezvous Calibration for Low-Cost Mobile Sensors. In *Proc. of ACM UbiComp/ISWC'23 Adjunct*. 688–693.
- [13] Georgios K Papageorgiou, Mathini Sellathurai, and Yonina C Eldar. 2021. Deep networks for direction-of-arrival estimation in low SNR. *IEEE Trans. Signal Process.* 69 (2021), 3714–3729.
- [14] Kunal Sankhe, Mauro Belgiovine, Fan Zhou, and et al. 2019. No radio left behind: Radio fingerprinting through deep learning of physical-layer hardware impairments. *IEEE Trans. Cogn. Commun. Netw.* 6, 1 (2019), 165–178.
- [15] Erik Sippel, Melanie Lipka, Johanna Geiß, and et al. 2019. In-situ calibration of antenna arrays within wireless locating systems. *IEEE Trans. Antennas Propag.* 68, 4 (2019), 2832–2841.
- [16] Haoyang Wang, Xuecheng Chen, Yuhuan Cheng, Chenye Wu, Fan Dang, and Xinlei Chen. 2022. H-SwarmLoc: Efficient Scheduling for Localization of Heterogeneous MAV Swarm with Deep Reinforcement Learning. In *Proc. of ACM SenSys'22*. 1148–1154.
- [17] Martin Woolley. 2019. Bluetooth core specification v5. 1. In *Bluetooth*.
- [18] Chengzhao Yu, Ji Luo, Rongye Shi, and et al. 2022. ST-ICM: spatial-temporal inference calibration model for low cost fine-grained mobile sensing. In *Proc. of ACM MobiCom'22*. 910–912.
- [19] Junqing Zhang, Sekhar Rajendran, Zhi Sun, and et al. 2019. Physical layer security for the Internet of Things: Authentication and key generation. *IEEE Wirel. Commun.* 26, 5 (2019), 92–98.
- [20] Xinwei Zhang, Guyue Li, Junqing Zhang, and et al. 2021. Deep-learning-based physical-layer secret key generation for FDD systems. *IEEE Internet Things J.* 9, 8 (2021), 6081–6094.
- [21] Yawen Zheng, Fan Dang, Zihao Yang, and et al. 2024. BlueKey: Exploiting Bluetooth Low Energy for Enhanced Physical-Layer Key Generation. In *Proc. of IEEE INFOCOM'24*.